Size Analysis of PDMS−Magnetite Nanoparticle Complexes: Experiment and Theory

O. Thompson Mefford,[†] M. R. J. Carroll,[‡] M. L. Vadala,[§] J. D. Goff,[†] R. Mejia-Ariza,[†] M. Saunders,[||] R. C. Woodward,[‡] T. G. St. Pierre,[‡] R. M. Davis,[†] and J. S. Riffle*,[†]

Macromolecules and Interfaces Institute, Virginia Tech, Blacksburg, Virginia 24061, Nanomedics, LLC, Erie, Pennsylvania 16509, and School of Physics and Center for Microscopy Characterisation and Analysis, The University of Western Australia, Crawley, Western Australia 6009, Australia

Received September 24, 2007. Revised Manuscript Received January 22, 2008

Biocompatible, hydrophobic nanoparticles show great promise as biomaterials. This paper reports the synthesis, magnetic separation, and characterization of magnetite nanoparticles with polydimethylsiloxane (PDMS) adsorbed onto their surfaces. The particle size distributions were narrowed by employing a magnetic separation/fractionation technique to remove larger particles and aggregates from an original distribution. A probability averaging method that incorporates particle size distributions of the magnetite cores derived from TEM is proposed, together with implementation of a polymer brush model for calculating the thickness of the polymer surfactant, for predicting the sizes and size distributions of these complexes in suspension. The intensity, volume, and number average size distributions in solution were predicted, and the values were compared to sizes of the complexes measured by DLS. This approach provides a tool for a more precise characterization of the size distributions of polymer−nanoparticle complexes relative to previous methods that utilized only a mean (single) core particle size. The predicted sizes of the complexes in dispersion closely approximate measured values from DLS for particles with narrow size distributions. Agreement between the predicted and measured sizes improves as the particle size distribution becomes narrower.

Introduction

Magnetic nanoparticles show great potential in a variety of biomedical applications. It has been demonstrated that they can have exceptional properties for MRI contrast enhancement, drug targeting and delivery, hyperthermia treatment, and magnetic separations of bioagents.[1,2] In addition, we have worked for several years to develop hydrophobic ferrofluids for treating retinal detachment.[3–7]

Magnetite nanoparticles were first produced in the 1960s by grinding iron oxides with surfactants and long chain hydrocarbons.[8] This was followed by the development of precipitation techniques utilizing reactions of soluble iron salts with base.[9,10] This method has been employed to create magnetite particles functionalized with a gamut of materials including water soluble polymers such as dextran[11] and poly(ethylene oxide),[12,13] to nonpolar materials such as polystyrene and poly(methyl methacrylate).[14] Other techniques have also proven successful for synthesizing magnetite nanoparticles. These include the use of microemulsions (i.e., reverse micellar solutions),[15–17] polyol reductions,[18,19] and elevated temperature decompositions of organic precursors.[20,21] Both Tartaj et al. and Harris et al. have presented reviews of these techniques.[2,22]

* Corresponding author. Address: 2018 Hahn Hall, Department of Chemistry, Virginia Tech, Blacksburg, VA 24061. Phone: (540) 231-8214. E-mail: judyriffle@aol.com.
[†] Virginia Tech.
[‡] School of Physics, The University of Western Australia.
[§] Nanomedics, LLC.
[||] Center for Microscopy Characterisation and Analysis, The University of Western Australia.

(1) Pankhurst, Q. A.; Connolly, J.; Jones, S. K.; Dobson, J. *J. Phys. D: Appl. Phys.* **2003**, *36*, R167.
(2) Tartaj, P.; Puerto-Morales, M. D.; Veintemillas-Verdaguer, S.; Gonzalez-Carreno, T.; Serna, C. J. *J. Phys. D: Appl. Phys.* **2003**, *36*, R182.
(3) Dailey, J. P.; Phillips, J. P.; Li, C.; Riffle, J. S. *J. Magn. Magn. Mater.* **1999**, *194*, 140.
(4) Stevenson, J. P.; Rutnakornpituk, M.; Vadala, M. L.; Esker, A. R.; Charles, S. W.; Wells, S.; Dailey, J. P.; Riffle, J. S. *J. Magn. Magn. Mater.* **2001**, *225*, 47.
(5) Vadala, M. L.; Zalich, M. A.; Fulks, D. B.; St. Pierre, T. G.; Dailey, J. P.; Riffle, J. S. *J. Magn. Magn. Mater.* **2005**, *293*, 162.
(6) Wilson, K. S.; Goff, J. D.; Riffle, J. S.; Harris, L. A.; St. Pierre, T. G. *Polym. Adv. Technol.* **2005**, *16* (2–3), 200.
(7) Mefford, O. T.; Woodward, R. C.; Goff, J. D.; Vadala, T. P.; St. Pierre, T. G.; Dailey, J. P.; Riffle, J. S. *J. Magn. Magn. Mater.* **2007**, *311*, 347.
(8) Papell, S. S. U.S. Patent 3 215 572, 1965.
(9) Reimers, G. W.; Khalafalla, S. E. U.S. Patent 3 843 540, 1974.
(10) Kelly, J. R. U.S. Patent 4 019 994, 1977.
(11) Molday, R. S. U. S. Patent 4 452 773, 1984.
(12) Suzuki, M.; Shinkai, M.; Kamihira, M.; Kobayashi, T. *Biotechnol. Appl. Biochem.* **1995**, *21*, 335.
(13) Harris, L. A.; Goff, J. D.; Carmichael, A. Y.; Riffle, J. S.; Harburn, J. J.; St. Pierre, T. G.; Saunders, M. *Chem. Mater.* **2003**, *15* (6), 1367.
(14) Noguchi, H.; Yanase, N.; Uchida, Y.; Suzuta, T. *J. Appl. Polym. Sci.* **1993**, *48* (9), 1539.
(15) Carpenter, E. E. *J. Magn. Magn. Mater.* **2001**, *225* (1–2), 17.
(16) Boutonnet, M.; Kizling, J.; Stenius, P. *Colloids Surf., A* **1982**, *5* (3), 209.
(17) Lopez-Quintela, M. A.; Rivas, J. *J. Colloid Interface Sci.* **1993**, *158* (2), 446.
(18) Viau, G.; Fievet-Vicent, F.; Fievet, F. *J. Mater. Chem.* **1996**, *6* (6), 1047.
(19) Viau, G.; Fievet-Vicent, F.; F., F. *Solid State Ionics* **1996**, *84*, 259.
(20) Sun, S.; Zeng, H. *J. Am. Chem. Soc.* **2002**, *124*, 8204.
(21) Park, J.; Lee, E.; Hwang, N.-M.; Kang, M.; Kim, S. C.; Hwang, Y.; Park, J.-G.; Noh, H.-J.; Kim, J.-Y.; Park, J.-H.; Hyeon, T. *Angew. Chem.* **2005**, *44*, 2872.

10.1021/cm702730p CCC: $40.75
Published on Web 03/04/2008

Magnetic separations have been explored for several decades. For instance, Watson described the removal of micrometer-sized paramagnetic particles with stainless steel wool in applied fields from 0.1 to 0.15 T.[23] This approach has been utilized by many researchers as it offers simplicity and a low-cost/high-throughput approach[24] that has recently been employed for separations of tagged cells. Sarikaya et al. have presented an excellent review of the design parameters (e.g., flow rate and strength of the applied field) for this type of particle separation in aqueous media.[25] An alternative to this technique is magnetic field-flow fractionation (MFFF). This method separates particles into various fractions due to the particles' individual magnetic moment.[24,26–30]

In this work, magnetite nanoparticles with terminally attached PDMS chains bound to their surfaces were synthesized for sterically stabilizing the nanoparticles against flocculation. The sizes and size distributions of the particles were adjusted by magnetically removing larger particles and aggregates via magnetic separation. This was achieved by passing dispersions of the particles through columns packed with granules of soft magnetic material. Characterization of the magnetite−PDMS complexes and their size distributions and properties will be discussed along with calculations of the polymer brush thicknesses and the hydrodynamic radii of the complexes in dispersions.

This paper outlines a general methodology for characterizing metal oxide particles that are sterically stabilized with polymer brushes even when the particle size distribution is not narrow. Nanoparticles to be utilized in a myriad of applications are typically polydisperse. For biomedical applications, sterically stabilizing polymer layers are frequently needed that can alter size due to brush thickness. It is important to quantify the size distributions of complexes for controlling drug delivery, dosage, cell uptake, and renal clearance. In addition, it is believed that size distributions of MRI contrast agents will be important for understanding and enhancing their effectiveness.

Experimental Section

Materials. Hexamethylcyclotrisiloxane (D_3, Gelest, Inc., 98%) was dried over calcium hydride and sublimed under a vacuum into preweighed, flame-dried, round-bottom flasks, each containing a magnetic stir bar. The flasks were purged with nitrogen and reweighed to determine the amount of D_3 in each flask. Cyclohexane (EM Science, 99%) was stirred with concentrated sulfuric acid for 48 h, washed with deionized water until neutral, stirred over magnesium sulfate and then over calcium hydride, distilled, stored over sodium under a nitrogen atmosphere, and freshly distilled prior to use. Tetrahydrofuran (THF, EM Science, 99.5%) was dried over calcium hydride, distilled, and stored over sodium in the presence of benzophenone under a nitrogen atmosphere until the solution was a deep purple. The THF was distilled just prior to use. Toluene (Burdick and Jackson, 99.9%) was washed twice with concentrated sulfuric acid and neutralized with water. It was dried over magnesium sulfate for 1 h and then over calcium hydride overnight and distilled just before use. Aqueous hydrochloric acid (50% by volume) was prepared by adding 5 mL of concentrated hydrochloric acid (EM Science) to 5 mL of deionized water in a graduated cylinder. Ferric chloride hexahydrate ($FeCl_3 \cdot 6H_2O$) and ferrous chloride tetrahydrate ($FeCl_2 \cdot 4H_2O$) (both from Aldrich) were stored under nitrogen in a desiccator and used as received. Iron granules (Alfa Aesar, 1–2 mm, 99.98%) were washed repeatedly with a variety of solvents to remove any coating on the surface. The granules were subsequently dried overnight in a vacuum oven at 40 °C. Ammonium hydroxide (Alfa Aesar, 50% v/v aqueous), chloroform (EM Science, 99.9%), octamethylcyclotetrasiloxane (D_4, Gelest, Inc.) mercaptoacetic acid (Aldrich, 97%), 2,2′-azobisisobutyronitrile (AIBN, Aldrich, 98%), *n*-butyllithium (1.6 M, Aldrich), trivinylchlorosilane (Gelest, Inc., 95%), and trimethylchlorosilane (Gelest, Inc., 99%) were used as received. NdFeB doughnut-shaped magnets that were magnetized through the thickness were purchased from Engineered Concepts. The field generated by the doughnut magnets was 0.24 T, and the magnets had dimensions of 1.0 in. (2.54 cm) O.D., 0.5 in. (1.27 cm) I.D, and 0.25 in. (0.635 cm) thickness.

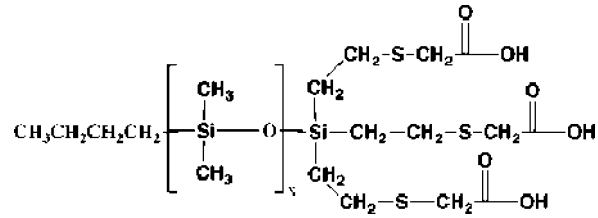

Figure 1. Tricarboxylic acid-functional PDMS

Synthesis of PDMS-Coated Magnetite Nanoparticles. Methods for synthesizing nanoparticles complexed with carboxylate-functional PDMS oligomers have been previously reported (Figure 1).[6,7] The PDMS oligomer that was utilized for the ferrofluid in the present work was a 3242 g mol^{-1} (M_n) PDMS dispersion stabilizer that was prepared by living polymerization. D_3 (51.23 g, 0.23 mol) was sublimed into a flame-dried, round-bottom flask. The flask was purged with nitrogen, and cyclohexane (50 mL) was added via a syringe. Once the D_3 monomer was dissolved at room temperature, 1.6 M *n*-butyllithium (10.86 mL, 0.0174 mol) was added to the reaction, and the solution was stirred for 0.5 h. THF (15 mL) was then charged to the solution as a reaction promoter. ^{1}H NMR was used to monitor the progress of the living anionic polymerization. At ∼95% conversion of monomer, the polymer was terminated with an excess of trivinylchlorosilane (3.78 mL, 0.0261 mol) and stirred overnight. The PDMS oligomer was diluted with chloroform and washed with deionized water (3×). The solution was concentrated under vacuum and poured into methanol to precipitate the liquid polymer. The polymer was dried under a vacuum at 80 °C overnight to remove residual monomer.

The thiol-ene addition of mercaptoacetic acid to the trivinylsilane-functional PDMS oligomer was conducted as follows. A 2800 g mol^{-1} trivinylsiloxy-terminated PDMS (15 g, 0.016 eq vinyl) was added into a flame-dried, round-bottom flask and dissolved in distilled toluene (25 mL). The reaction solution was deoxygenated by sparging it with nitrogen for 2 h. AIBN (3.7×10^{-3} g, 2.4×10^{-4} mol) and mercaptoacetic acid (1.67 mL, 0.024 mol) were

(22) Harris, L. A.; Riffle, J. S.; St. Pierre, T. G. *J. Aust. Ceram. Soc.* **2005**, *41* (2), 23.
(23) Watson, J. H. P. *J. Appl. Phys.* **1973**, *44* (9), 4209.
(24) Rheinlander, T.; Kotitz, R.; Weitschies, W.; Semmler, W. *J. Magn. Magn. Mater.* **2000**, *219*, 219.
(25) Sarikaya, M.; Abbasov, T.; Erdemoglu, M. *J. Dispersion Sci. Technol.* **2006**, *27*, 193.
(26) Rheinlander, T.; Roessner, D.; Weitschies, W.; Semmler, W. *J. Magn. Magn. Mater.* **2000**, *214*, 269.
(27) Espy, M. A.; Sandin, H.; Carr, C.; Hanson, C. J.; Ward, M. D., Jr *Cytometry, Part A* **2006**, *69A*, 1132.
(28) Carpino, F.; Moore, L. R.; Zborowski, M.; Chalmers, J. J.; Williams, P. S. *J. Magn. Magn. Mater.* **2005**, *293*, 546.
(29) Latham, A. H.; Feitas, R. S.; Schiffer, P.; Williams, M. E. *Anal. Chem.* **2005**, *77*, 5055.
(30) Kelland, D. R. *IEEE Trans. Magn.* **1998**, *34* (4), 2123.

added to the reaction vessel, and the flask was purged with nitrogen. The reaction was heated to 80 °C and stirred for 1 h. Reaction completion was confirmed by observing the disappearance of the vinyl proton peaks at ~6 ppm in the ^{1}H NMR spectra. The solvent was removed under vacuum, and the polymer was stirred in methanol (30 mL) for 30 min. Deionized water was added to the solution until the polymer coagulated into a solid, and it was then collected via filtration. The methanol/deionized water coagulation process was repeated several times (5X), and the polymer was dried under vacuum at 80 °C. The M_n of the functionalized PDMS oligomer was determined to be 3242 g mol^{-1} by ^{1}H NMR.

A preparative method for a 50:50 wt:wt PDMS stabilizer: magnetite complex is provided. Magnetite was synthesized using a chemical precipitation of iron salts after reaction with base. Iron(III) chloride hexahydrate (2.01 g, 7.44×10^{-3} mol) and iron(II) chloride tetrahydrate (0.736 g, 3.70×10^{-3} mol) were weighed into separate round-bottom flasks and each was dissolved in 20 mL of deoxygenated water. The two iron salt solutions were added to a 500 mL, three-necked, round-bottom flask connected to a mechanical stirrer. Ammonium hydroxide (15 mL) was added via syringe until the rapidly stirring solution turned black and reached a pH of 9–10. The 3242 g mol^{-1} PDMS dispersion stabilizer (0.86 g) was dissolved in dichloromethane (20 mL) and added to the basic magnetite dispersion. After the solution was stirred for 30 min, 50 vol % aqueous hydrochloric acid (~6 mL) was added slowly until the solution became slightly acidic (pH 5–6). The acidic interfacial solution was stirred for 1 h, then the dichloromethane was removed under a vacuum. The magnetite complex was collected with a magnet and the water was decanted. The magnetite complex was washed several times with water (5×) and methanol (5×) before drying overnight at 40 °C under reduced pressure. This produced the material that was used as the feedstock for the magnetic separations.

Magnetic Separation of PDMS-Coated Magnetite Nanoparticles. Magnetic separation columns were comprised of ~6 g of soft iron granules firmly packed into 3 mL plastic syringes. A magnetic field of 0.24 T was generated by a NdFeB doughnut-shaped magnet placed around the exterior of the syringe. PDMS-coated magnetite nanoparticles were diluted in chloroform to a concentration of 0.002 mg mL^{-1}. The dispersion was sonicated with a Biologics ultrasonic homogenizer (model 150V/T) for 5 min using the 50% power setting with a microtip probe and a 50% pulse cycle. Following sonication, 150 mL of the chloroform dispersion (0.3 g of particles) was passed through the column at a flow rate of ~20 mL min^{-1} and collected. Alternatively, 150 mL of the chloroform dispersion was passed through 5 freshly prepared separation columns in series with a donut magnet around each syringe. The positions of the separation columns were adjusted such that the donut-shaped magnets were approximately 10 cm apart to prevent strong magnetic interaction. The collected dispersions were dried under vacuum and weighed to determine the amount of material that had been retained in the separation columns.

Characterization. *Thermogravimetric Analysis (TGA).* TGA was carried out on the PDMS-coated magnetite nanoparticles using a TA Instruments TGA Q500. After first equilibrating the samples at 30 °C, the temperature was ramped at 10 °C min^{-1} to a maximum of 700 °C under a nitrogen purge. Char yields (the mass remaining at the end of the experiments) were recorded at the maximum temperature.

Transmission Electron Microscopy (TEM). TEM was conducted with a JEOL 3000F field-emission-gun transmission electron microscope (operated at 300 kV) equipped with a 1024 × 1024 pixel digital imaging system. Dry samples of the magnetite complexes were dispersed in chloroform and cast onto amorphous carbon-coated copper grids for analysis. Great care was taken to ensure that both eucentric height and focus were set consistently from one sample to another in order to reduce uncertainty in the digital image analyses. Images were acquired at a magnification of 300 kx, corresponding to 1.65 pixels nm^{-1}. This magnification gave both sufficient resolution and contrast for digital image analysis, and provided a large enough field of view to obtain adequate numbers of particles. Particle size analysis was performed using Reindeer Graphics' Fovea Pro 4 plug-in for Adobe Photoshop CS2. Mean and standard deviations of the particle size diameters were calculated based upon 3500–5000 particles per sample, and particle size distributions were fitted with a Weibull distribution.

Superconducting Quantum Interference Device (SQuID). Magnetic properties were measured using a 7-T Quantum Design MPMS SQuID magnetometer. Hysteresis loops on dried samples of the magnetite-polymer complexes were performed in fields of up to 7 T at 300 and 5 K. The 5 K hysteresis loop was obtained to determine the coercivity and saturation magnetization, and to observe the presence or absence of any exchange bias. Samples of the PDMS-coated magnetite particles were mobile at temperatures as low as 170 K (the glass transition temperature of the PDMS is approximately 150 K).[31,32] To reduce Brownian reorientation of the particles, we mixed the samples with molten wax and then allowed them to cool; this produced a solid sample at 300 K. Zero-field-cooled/field-cooled measurements were performed on these samples in a field of 0.01 T.

Dynamic Light Scattering (DLS). DLS measurements were conducted with a Malvern Zetasizer ZS compact scattering spectrometer (Malvern Instruments Ltd., Malvern, UK) at a wavelength of 633 nm from a 4.0 mW, solid-state He−Ne laser at a scattering angle of 170°. Intensity average, volume average, and number average diameters were calculated from the autocorrelation function using Malvern's Zetasizer Nano 4.2 software utilizing a version of the CONTIN algorithm.[33]

Results and Discussion

Synthesis and Separation of Magnetic Nanoparticles. PDMS-coated magnetite nanoparticles have been prepared with different sizes to compare techniques for size analysis and test theoretical predictions of size distributions. Magnetite was synthesized by reacting a stoichiometric ratio of iron chloride salts with hydroxide. The surfaces of the magnetite nanoparticles were coated by adsorbing a PDMS oligomer that had three carboxylates on one end and a nonfunctional trimethylsilyl group at the other (Figure 1). The isoelectric point of magnetite in water is pH ~6.8, so at pH 6, there is a net positive charge on the metal oxide surface. The isoelectric point of magnetite has been confirmed by measurements of the zeta potentials by a number of authors using a variety of electrolytes including $NaClO_4$,[34] $NaNO_3$,[35] and H_2SO_4 to vary pH.[36] It is reasoned that the PDMS adsorbs through electrostatic binding of the negatively charged carboxylate end group onto cationic sites on the

(31) Miller, G. W.; Saunders, J. H. *J. Appl. Polym. Sci.* **1969**, *13* (6), 1277.
(32) Helmer, J. D.; Polmanteer, K. E. *J. Appl. Polym. Sci.* **1969**, *13* (10), 2113.
(33) *Calculating Volume Distribution From Dynamic Light Scattering*; Malvern Instruments: Worcestershire, U.K., 2007.
(34) Sun, Z.-X.; Su, F.-W.; Forsling, W.; Samskog, P.-O. *J. Colloid Interface Sci.* **1998**, *197*, 151.
(35) Viota, J. L.; Vicente, J. D.; Duran, J. D. G.; Delgado, A. V. *J. Colloid Interface Sci.* **2005**, *284*, 527.
(36) Caba, B. Brush-Forming Copolymers on Magnetite Nanoparticles. Ph.D. Dissertation, Virginia Tech, Blacksburg, VA,2007.

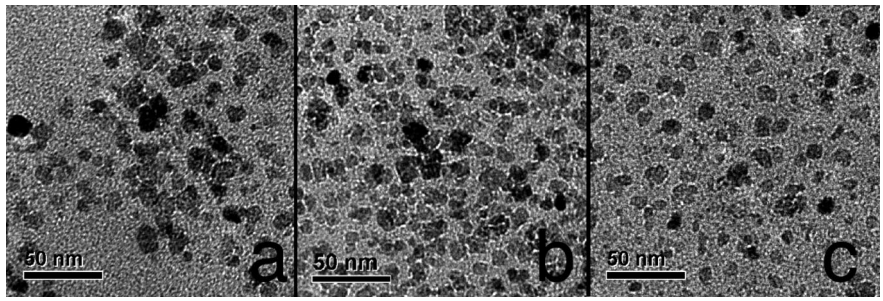

Figure 2. TEM images of PDMS−magnetite particles that were (a) not magnetically separated, (b) passed through a single separation column, and (c) passed through five separation columns.

Table 1. Composition from TGA, Magnetite Size and Standard Deviation from TEM, Saturation Magnetization (M_s) at 5 K of PDMS−Magnetite Complexes

sample name	PDMS−magnetite complex	wt % magnetite	mean magnetite diameter (nm)	standard deviation (nm)	M_s @ 5 K (Am^2/kg)
0-pass	original sample – not magnetically separated	58	10.4	5.6	78.6
1-pass	passed through a single separation column	43	7.7	4.2	57.4
5-pass	passed through 5 magnetic separation columns	20	4.5	2.3	39.1

magnetite surface, and that the nonfunctional end of the PDMS oligomer provides a brush layer that extends outward from the nanoparticle to prevent aggregation. Following adsorption, the particles were extracted with methanol (a solvent for the carboxylate-functional PDMS) to remove any unbound polymer.

To remove aggregates and large particles, dispersions of the PDMS-coated magnetite particles in chloroform were passed through magnetic separation columns. Size distributions were compared among complexes that had not been magnetically separated, complexes that passed through a single separation column (with ∼60 wt % yield), and complexes that passed through a series of five separation columns (with ∼40 wt % yield). All of the complexes were extracted with methanol to remove any residual unbound polymer that might have passed through the separation column, and then the magnetic complexes were collected with a magnet.

The sizes of these polymer-magnetite complexes in dispersions reflect the densities of oligomeric chains on their surfaces, the molecular weights of the chains, and their propensity to interact with the solvent. The particle-polymer compositional ratios were determined by weight loss measurements (TGA). The materials were heated under nitrogen in a TGA furnace past the point of thermal degradation of the PDMS brushes, and this left only the magnetite mass as residual char. As previously reported, PDMS leaves no detectable char above 650 °C when heated under these conditions.[37] It has also been shown previously that the magnetite does not lose weight under the conditions utilized in these measurements.[38] The materials that had been magnetically separated had lower concentrations of magnetite compared to the original material (Table 1). Because of their larger magnetic moments, larger particles and aggregates are more likely to be entrapped by the separation column. Since the separations preferentially removed aggregates and larger particles, complexes that passed through the columns should have higher magnetite specific surface areas, leading to higher mass fractions of polymer in the eluted materials.

Analysis of the Sizes of the Magnetite Cores by TEM. Dispersions of PDMS-coated magnetite particles were cast onto carbon grids and analyzed via TEM. The samples that had been magnetically separated had lower fractions of aggregates (Figure 2), but further interpretation with only a visual inspection of the micrographs was inconclusive.

Size analyses were performed to determine the distributions of the diameters of the magnetite cores of the particles. Typically, 4–6 TEM images were analyzed for each sample, resulting in about 4000 particles being measured. Images were blurred slightly (typically 1–2 pixels) to flatten noise in the background, and then an intensity threshold was applied to distinguish the particles from the background. Fovea Pro's watershed tool was then used to distinguish particles that were close together but not connected. Before measuring the sizes of the particles, the original image was manually compared to the threshold image to check for any discrepancies, and all of the detected errors were manually corrected on the threshold image. This ensured that only true particles were identified in the images and any potential artifacts were removed prior to analysis. The arithmetic means and standard deviations of the distributions were calculated from the data (Table 1). It was found that the particle size distributions of all three samples could be accurately represented by a two-parameter Weibull distribution (Figure 3). The expression for the Weibull distribution is

$$P(r) = \frac{\gamma}{\alpha}\left(\frac{r}{\alpha}\right)^{\gamma-1}\exp\left(\frac{-r}{\alpha}\right)^{\gamma} \quad (1)$$

where $P(r)$ is the probability of a particle with radius r, α is a scale parameter, and γ is a shape parameter.[39] Magnetic separations resulted in particles that were smaller and had

(37) Jovanovic, J. D.; Govedarica, M. N.; Dvornic, P. R.; Popovic, I. G. *Polym. Degrad. Stab.* **1997**, *61*, 87.

(38) Zhang, Q.; Thompson, M. S.; Carmichael, A. Y.; Caba, B. L.; Zalich, M. A.; Lin, Y. N.; Mefford, O. T.; Davis, R. M.; Riffle, J. S. *Langmuir* **2007**, *23*, 6927.

(39) Bury, K. V. *Statistical Models in Applied Science*; Robert E. Krieger Publishing Company: Malabar, FL, 1986.

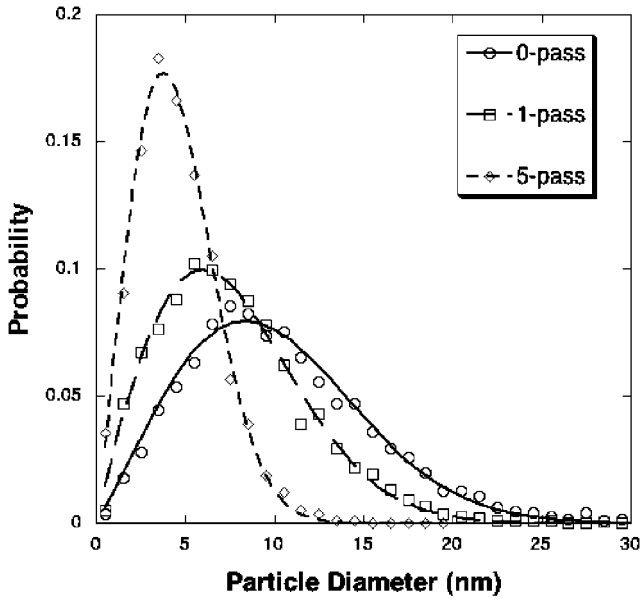

Figure 3. Weibull (number based) probability distribution functions of the magnetite core sizes fitted to particle diameters obtained from TEM.

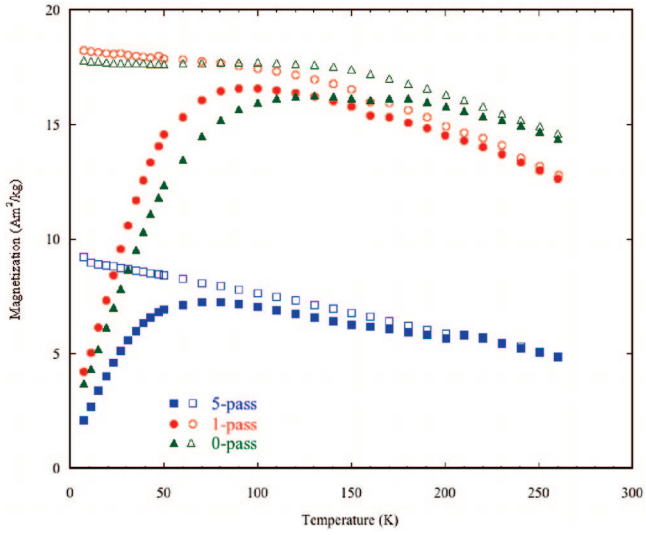

Figure 4. Zero-field-cooled (closed symbols)/field-cooled (open symbols) magnetization curves.

narrower distributions (Figure 3). Moreover, multiple passes through the separation columns produced smaller average sizes and narrower distributions.

Magnetic Properties of the PDMS−Magnetite Nanoparticle Complexes. Zero field cooled-field cooled (ZFC-FC) curves on the dried complexes showed sudden changes in magnetization at 170 and 230 K. These changes were thought to be associated with changes in the rheological properties of the PDMS surfactant, where the particles undergo Brownian rotation as the sample heats through transition temperatures corresponding to the PDMS in the complexes. In order to reduce these effects, the samples were embedded in a wax to fix the orientation of the PDMS-coated magnetite. The ZFC-FC curves for the fixed samples are shown in Figure 4. Although the artifacts associated with the Brownian rotation were reduced, they were not eliminated, particularly in the case of the material that had been passed through five separation columns (the so-called 5-pass

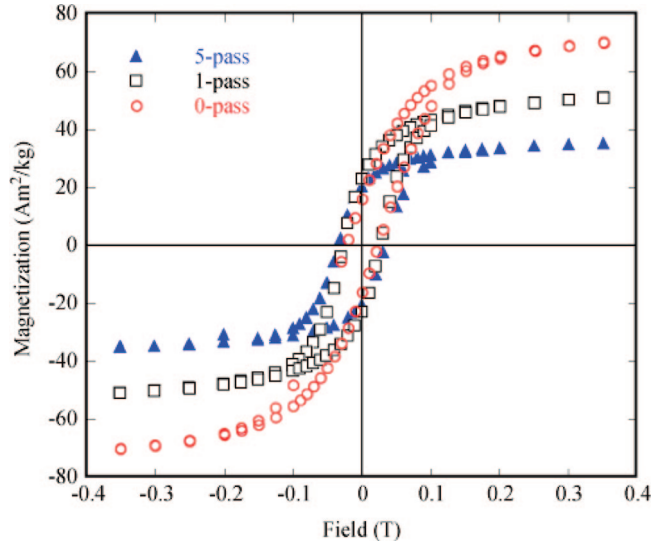

Figure 5. The 5 K hysteresis loops show minimal coercivity, zero exchange bias, and a decreasing saturation magnetization with increasing numbers of magnetic separations.

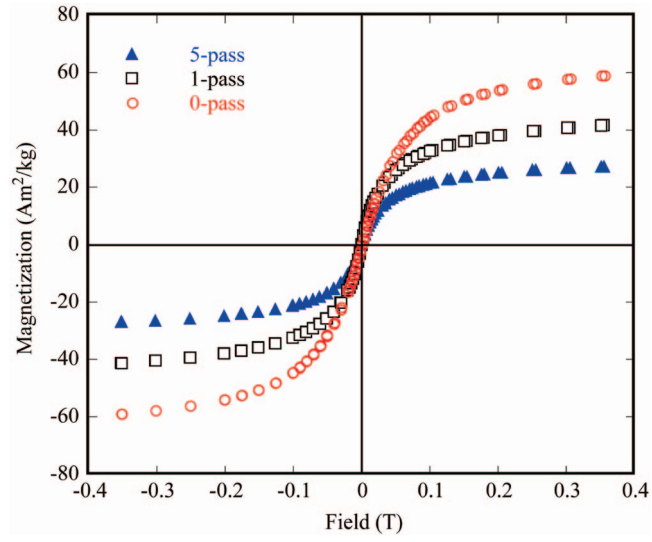

Figure 6. 300 K hysteresis loops show no hysteresis and a decrease in the saturation magnetization with increasing magnetic separation.

sample). This may be due to a partial segregation of the complex and wax during freezing of the wax, resulting in phases of relatively pure complex. The ZFC-FC curves of both the 0-pass and 1-pass samples do not close, and this suggests the presence of some ferromagnetic particles, possibly in the form of aggregates. The curves for the 5-pass sample closed at a temperature of 210K, but this corresponds to a rotational artifact in both the zero-field-cooled and field-cooled curves and may not be a true representation of the maximum blocking temperature. There was not, however, any evidence for a significant ferromagnetic contribution in this sample at higher temperature as can be seen in the ZFC-FC curves for the 0-pass and 1-pass samples. This demonstrates that the magnetic separation technique is an efficient method of removing larger particles and aggregates.

Hysteresis loops measured at 5 and 300 K are shown in Figures 5 and 6, respectively. The values of specific magnetization given in the figures have been corrected to reflect the magnetization of the magnetite particles (i.e., Am^2

Table 2. Comparison of Diameters of the Complexes in Suspension Derived from Chain Extension Theory in Combination with TEM (for the Core Sizes) and Experimental Values from DLS of the Volume Average Diameter of the PDMS−Magnetite Complexes[a]

PDMS−magnetite sample	avg. no. of chains/nm^2 $\bar{\sigma}$ (eq 2)	intensity avg. diameter measured (DLS)	intensity avg. diameter calcd (eq 7)	volume avg. diameter measured (DLS)	volume avg. diameter calcd (eq 8)	no. avg. diameter measured (DLS)	no. avg. diameter calcd (eq 14)
0-pass	0.79	53.3 ± 1.5	27.6	36.4 ± 2.1	24.9	29.0 ± 2.1	19.9
1-pass	0.77	49.9 ± 5.3	23.6	33.8 ± 1.0	21.3	26.2 ± 2.1	17.0
5-pass	1.93	35.8 ± 1.8	18.9	22.5 ± 0.4	17.6	17.0 ± 0.7	14.9

[a] Note all diameters are in units of nanometers.

per kg of Fe_3O_4). Analysis of the 5K hysteresis loops shows that all three materials have coercivities of ~250 Oe (as expected for magnetite particles) and no sign of any enhanced coercivity or exchange bias which might indicate the presence of coupled magnetic phases or significant disorder within the particles. Saturation magnetization was calculated by subtracting the diamagnetic contribution as inferred from the slope of the hysteresis curve at high fields. The saturation magnetization of the magnetite declines with increasing numbers of magnetic separation passes which correlates to a decrease in average particle size (Table 1). Such a decrease in magnetization with average particle size in this small size range is well-documented in the literature.[40,41]

The magnetization curves for the samples at 300K show no sign of hysteresis. This is as expected, since at 300 K, the samples are viscous liquids in which any ferromagnetic particles undergo Brownian rotation and will rapidly align with the applied field.

Calculation of Chain Density and Particle Functionality. The average chain density, $\bar{\sigma}$ the number of chains per nm^2 of magnetite surface), was calculated using the Weibull probability functions of the magnetite core sizes from TEM image analysis, and compositions of the complexes from TGA according to

$$\bar{\sigma} = \frac{W_{\mathrm{PDMS}} N_{\mathrm{Av}} \rho_{\mathrm{mag}}}{M_{\mathrm{n}} W_{\mathrm{mag}}} \int_0^\infty \left(\frac{3}{r}\right) P(r)\, \mathrm{d}r \qquad (2)$$

where W_{PDMS} and W_{mag} are the mass fractions of the complex that consists of PDMS and magnetite, respectively, ρ_{mag} is the density of magnetite (5.17 g mL^{-1}),[42] M_{n} is the number average molecular weight of the PDMS chains, and N_{av} is Avogadro's number. The ratio (3/r) in the integral arises from the area/volume ratio for a sphere. The average functionality (number of chains per particle), $f(r)$, of a particle of given radius is then

$$f(r) = 4\pi r^2 \bar{\sigma} \qquad (3)$$

The calculated values for the PDMS-coated magnetite complexes (Table 2) indicate that the particles that were magnetically separated have more chains per area than the complex that was not magnetically separated. Thus, it is likely that by removing the clustered particles from the ensemble, a more discrete distribution that can be more efficiently coated with a higher chain density is produced.

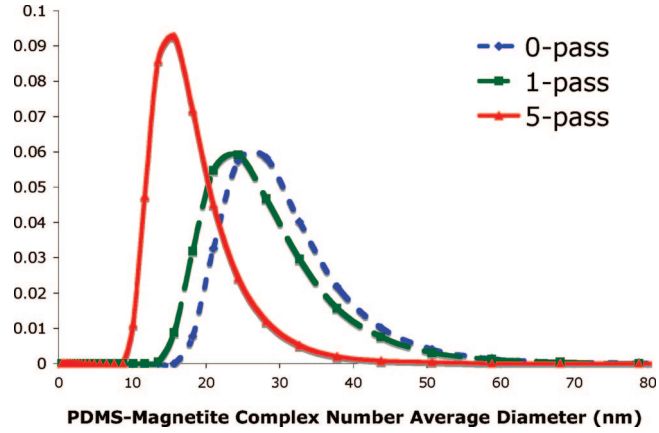

Figure 7. Number average hydrodynamic diameters of the PDMS−magnetite nanoparticles in chloroform from DLS indicate that particles that had been magnetically separated were smaller than those that had not been separated.

In addition, the increased curvature of a smaller particle may allow for a higher chain density.

Analysis of the Sizes of the PDMS−Magnetite Nanoparticles by DLS. The hydrodynamic diameters of the PDMS−magnetite nanoparticles were measured by DLS. The nanoparticle complexes were diluted with chloroform, which is a good solvent for PDMS.[43] Consistent with the core sizes derived from TEM, materials that had been magnetically separated had smaller diameters and narrower distributions in solution (Table 2). The probability size distribution curves constructed from the TEM and DLS data (Figures 3 and 7, respectively) have similar shapes, and the material that had been rigorously separated through five magnetic separation columns had a narrower size distribution when analyzed by either method relative to the other two samples. It was expected that the DLS-based sizes would be larger than the TEM values, since DLS measures the size of both the magnetite cores and the PDMS coronas, while the TEM images only the magnetite cores. Moreover, because the chloroform dispersion medium is a good solvent for PDMS, the positive interaction between the PDMS chains and the medium would also be expected to increase the sizes, and this would be reflected in the DLS measurements.

Predicted Sizes of the Nanoparticle Complexes in Dispersions. We have developed a method for applying chain extension theory to predict corona sizes around the magnetite cores.[38] This was utilized in combination with TEM size distributions of the magnetite cores to arrive at predicted sizes for these complexes in dispersion. The predicted solution sizes derived from combined experimental and theoretical values were then compared to experimental

(40) Morales, M. P.; Andres-Verges, M.; Veintemillas-Verdaguer, S.; Montero, M. I.; Serna, C. J. *J. Magn. Magn. Mater.* **1999**, *203*, 146.
(41) Goya, G. F.; Berquo, T. S.; Fonseca, F. C.; Morales, M. P. *J. Appl. Phys.* **2003**, *94* (5), 3520.
(42) *CRC Handbook of Chemistry and Physics*, 87th ed.; CRC Press: Boca Raton, FL, 2006.
(43) Lee, J. N.; Park, C.; Whitesides, G. M. *Anal. Chem.* **2003**, *75*, 6544.

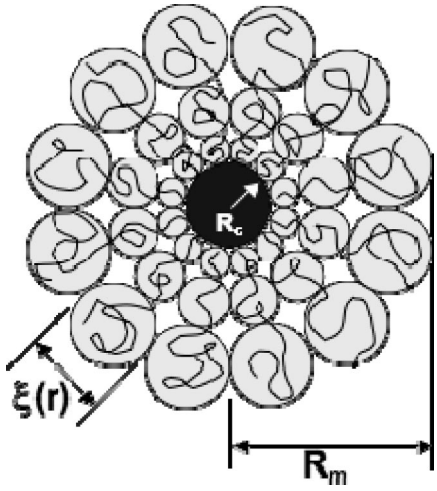

Figure 8. Representation of the PDMS-magnetite nanoparticle complex showing the Vagberg model parameters. Adapted from Daoud and Cotton.[45]

DLS data (Table 2). The sizes of the polymer-magnetite complexes were predicted with a density distribution (DD) model developed by Vagberg et al. (Figure 8).[44] This model, based on a model for star polymers by Daoud and Cotton,[45] assumes concentric shells with a constant number of blobs in each shell. The blob diameter ζ(r) is a continuous function of distance from the surface. The segment density in the shell varies with distance from the core that, in the present case, is the surface of the magnetite particle.

The DD model predicts the radius R_m of the PDMS−magnetite complex as a function of the core magnetite radius.

$$R_m(r) = \left(\frac{8N_k f(r) \frac{1-\upsilon}{2\upsilon}}{3 \cdot 4^{1/\upsilon} \upsilon} L_k + r^{1/\upsilon} \right)^{\upsilon} \tag{4}$$

where N_k is the number of Kuhn segments in one of the corona chains (a PDMS chain in the present case), ν is the Flory exponent, r is the radius of the magnetite particle, and $f(r)$ is the number of corona chains per particle that was calculated using equation 3. The Flory exponent, ν, was varied between 0.5 and 0.6 to address the polymer–solvent interactions for the two solvents that were investigated, D_4 and chloroform, respectively. Because of the chemical similarity between D_4 and PDMS, it was assumed that the polymer retains its unperturbed dimensions in D_4 (i.e., theta conditions). By contrast, chloroform is a good solvent for PDMS. The statistical segment or Kuhn length L_k is defined as

$$L_k = c_\infty l_0 \tag{5}$$

and the number of statistical segments in a chain, N_k, is defined as

$$N_k = n/c_\infty \tag{6}$$

where c_∞ is the characteristic ratio (5.2 for PDMS[44]), l_0 is the average length of a backbone bond (0.155 nm for PDMS), and n is the number of backbone bonds in a chain (2*degree of polymerization for PDMS).

The number average diameter, $\overline{D_n}$, of the nanoparticle complex can be calculated as

$$\overline{D_n} = 2\int_0^\infty P(r) R_m(r)\, dr \tag{7}$$

The volume average diameter, $\overline{D_v}$, was determined by a moment weighted method[46]

$$\overline{D_v} = \frac{2\int_0^\infty P(r) R_m^4(r)\, dr}{\int_0^\infty P(r) R_m^3(r)\, dr} \tag{8}$$

The intensity average diameter, $\overline{D_I}$, was determined using a method developed by Johnson and Prud'homme.[47] In dynamic light scattering, the particle sizes can be determined by first describing the relationship between the first cumulant, $\Gamma(q)$, and the scattering from a distribution of particles.

$$\frac{\Gamma(q)}{q^2} = \frac{\sum_{j=1}^{\infty} n_j I_j D_j}{\sum_{j=1}^{\infty} n_j I_j} \tag{9}$$

where q is the wave vector, n_j is the number of particles at a particular radius r_j, I_j is the scattering intensity from these particles, and D_j is the diffusion coefficient.[48] The diffusion coefficient, D_0, for the particles can be described in terms of the first cumulant and the Stokes–Einstein relation

$$D_0 = \frac{\Gamma(q)}{q^2} = \frac{k_B T}{6\pi\mu r} \tag{10}$$

where k_B is Boltzmann's constant, T is temperature in Kelvin, and μ is the viscosity of the solvent. Combining eqs 9 and 10, the intensity average radius, $\overline{R_I}$, can be described in terms of

$$\frac{6\pi\mu\overline{R_I}}{k_B T} = \frac{\sum_{j=1}^{\infty} n_j I_j}{\sum_{j=1}^{\infty} n_j I_j \frac{k_B T}{6\pi\mu R_j}} \tag{11}$$

The hydrodynamic radius of the particles was shown by DLS to be on the order of 30 nm. Therefore these particles should be in the Rayleigh scattering range in which the scattering intensity, $\overline{I_j}$, can be described as

$$I_j = I_0 q^4 \cos^2\theta \left[\left(\frac{n_p}{n_s} \right)^2 - 1 \right]^2 \frac{R_j}{9\beta^2} F_f(\theta) \tag{12}$$

where I_0 is the incident light intensity, θ is the scattering angle, n_p and n_s are the refractive indices of the particle and the solvent respectively, β is the distance from the particle to the light detector, and $F_f(\theta)$ is the Rayleigh form factor.[49] The scattering intensity is directly related to the radii of the particles to the sixth power, and thus eq 11 reduces to

(44) Vagberg, L. J. M.; Cogan, K. A.; Gast, A. P. *Macromolecules* **1991**, *24*, 1670.
(45) Daoud, M.; Cotton, J. P. *J. Phys. (Paris)* **1982**, *43* (3), 531.
(46) Allen, T. *Particle Size Measurement*, 3rd ed.; Chapman and Hall: London, 1981.
(47) Liu, Y.; Kathan, K.; Saad, W.; Prud'homme, R. K. *Phys. Rev. Lett.* **2007**, *98*, 036102.
(48) Russel, W. B.; Saville, D. A.; Schowalter, W. R. *Colloid Dispersions*; Cambridge University: Cambridge, U.K., 1987.
(49) Fuller, G. G. *Optical Rheometry of Complex Fluids*; Oxford University Press: New York, 1995.

$$\overline{R_I} = \frac{\sum_{k=1}^{\infty} n_k R_k}{\sum_{k=1}^{\infty} n_k R_k} \tag{13}$$

For a particle size distribution described by the Weibull probability function, the discrete summations in eq 13 can be replaced by integrals to calculate the intensity average diameter $\overline{D_I}$ as

$$\overline{D_I} = 2\overline{R_I} = 2\frac{\int_0^{\infty} P(r) R_m(r)^6 \, dr}{\int_0^{\infty} P(r) R_m(r)^5 \, dr} \tag{14}$$

Calculations were made for the number, volume, and intensity average sizes using eqs 7, 8, and 14, respectively, for the three samples and compared to the DLS values (Table 2). In all cases, the predicted values of the nanoparticle complex diameters vary in the expected order: intensity average > volume average > number average. Overall, the sizes measured by DLS, while larger, followed a similar trend to the values calculated from the TEM and compositional results in combination with the chain extension predictions. It should be noted that several classical problems arise in analyzing particle size distributions by DLS. First, transformation of the autocorrelation function to a size distribution is mathematically nonunique. Second, in the Rayleigh regime, the intensity of the scattered light is proportional to particle radius to the sixth power. Thus, the scattering for particles in the larger part of the distribution can complicate detection of scattering from smaller particles. This problem is less severe as the particle size distribution narrows. Our proposed method for predicting polymer−nanoparticle size distributions in dispersions couples a proven polymer brush model with TEM-based sizes of the magnetite cores, allowing one to calculate any moment of the size distribution.

The closest agreement was for the most narrow particle size distribution (five times magnetically separated) involving the volume and the number averages, the averages that give the least weight to aggregates in the distributions. Thus, the effects of any errors in calculating or estimating the size distribution are smallest with the calculated number average, larger with the volume average and largest with the intensity average. It is likely that samples with narrower size distributions would fit this model better than those with larger polydispersity. It is also likely that some larger particles and aggregates were not fully included in the TEM image analysis as they are difficult to image. This would result in lower predicted values.

Conclusions

PDMS−magnetite nanoparticle complexes were synthesized and magnetically separated, and this produced different size distributions. The complexes that were magnetically separated were smaller and had narrower size distributions than those that were not magnetically separated. TEM and DLS showed similar trends in distributions of the magnetite cores and sizes of the complexes as a function of the degree of magnetic separation, and this permitted us to utilize measurements of core size distributions to predict sizes of the complexes in dispersions. A careful experimental analysis by TEM of the size distributions of the magnetite cores was combined with the assumption that the surface chain density was constant. This was then utilized with a polymer brush model that was originally developed for star polymers to predict the distributions of particle sizes in dispersions. This approach provides a tool for a more precise characterization of the size distributions of polymer−nanoparticle complexes, relative to previous methods that utilized only a mean (single) core particle size.

It is critical that one be able to characterize the distributions of particle sizes in order to predict the stabilities of polymer−nanoparticle complexes in dispersions, because the interparticle potentials depend on the size distributions. While it is not yet clear how to fully account for the effect of size distribution on the separate van der Waals, steric, electrostatic and magnetic potentials, the ability to predict the size distributions is a necessary first step toward developing an understanding of these dependencies. Moreover, the rheological properties of neat fluids comprised of polymer−nanoparticle complexes, such as those investigated in this work, depend strongly on the larger particles in the distributions. In terms of applications for nanoparticles as drug delivery vehicles, pharmaceutical scientists will likely need to quantify the fractions of particles that are below or above a critical size to avoid clearance via the kidneys or clogging of capillary blood vessels. With some modifications this model could be applied to other nanoparticles that are coated with polymers and surfactants, allowing scientists and engineers to approximate the sizes and distributions of newly developed nanoparticles. In addition, these calculations could be extended to calculating the steric interaction forces between particles to aid in predicting the stabilities of nanoparticle suspensions.

Acknowledgment. The authors are grateful for the financial support of the NSF/ARC Materials World Network for the Study of Macromolecular Ferrofluids (DMR-0602932 and LX0668968), the National Eye Institute of the NIH under SBIR Contract B6867G1 and the ARC Discovery Grant DP0559333. Transmission electron microscopy was carried out using the facilities at the Centre for Microscopy, Characterisation and Analysis, The University of Western Australia, which is supported by University, State, and Federal Government funding.

CM702730P